Article

Synthesis and Characterization of Zero-Valent Fe-Cu and Fe-Ni Bimetals for the Dehalogenation of Trichloroethylene Vapors

Clarissa Settimi [1], Daniela Zingaretti [1,*], Simone Sanna [1], Iason Verginelli [1], Igor Luisetto [2], Antonello Tebano [1] and Renato Baciocchi [1]

[1] Department of Civil Engineering and Computer Science Engineering, University of Rome "Tor Vergata", Via del Politecnico 1, 00133 Rome, Italy; settimi@ing.uniroma2.it (C.S.); sanna@ing.uniroma2.it (S.S.); verginelli@ing.uniroma2.it (I.V.); tebano@ing.uniroma2.it (A.T.); baciocchi@ing.uniroma2.it (R.B.)

[2] Department of Energy Technologies and Renewable Sources, ENEA Research Center, Casaccia, Via Anguillarese 301, 00123 Rome, Italy; igor.luisetto@enea.it

* Correspondence: zingaretti@ing.uniroma2.it; Tel.: +39-06-72597741; Fax: +39-06-72597021

Abstract: In this study, zero-valent iron-copper (Fe-Cu) and iron-nickel (Fe-Ni) bimetals were prepared by disc milling for the dehalogenation of trichloroethylene vapors. For both Fe-Ni and Fe-Cu, three combinations in terms of percentage of secondary metal added were produced (1%, 5%, 20% by weight) and the formation of the bimetallic phase by milling was evaluated by X-ray diffraction (XRD) analysis. The disc milled bimetals were characterized by a homogenous distribution of Ni or Cu in the Fe phase and micrometric size visible from scanning electron microscopy with energy dispersive X-ray spectroscopy (SEM-EDS) analysis and by a relatively low specific surface area (0.2–0.7 m^2/g) quantified by the Brunauer–Emmett–Teller (BET) method. The reactivity of the produced bimetals was evaluated by batch degradation tests of TCE in the gas phase with 1 day of reaction time. Fe-Ni bimetals have shown better performance in terms of TCE removal (57–75%) than Fe-Cu bimetals (41–55%). The similar specific surface area values found for the produced bimetals indicated that the enhancement in the dehalogenation achieved using bimetals is closely related to the induced catalysis. The obtained results suggest that ZVI-based bimetals produced by disc milling are effective in the dehalogenation of TCE vapors in partially saturated conditions.

Keywords: zero-valent iron; bimetallic; disc milling; dechlorination; chlorinated solvent vapors

1. Introduction

Zero-valent iron (ZVI) is a reducing agent that has proven to be effective in the treatment of sites contaminated by several chlorinated solvents [1]. ZVI is easily available, and sustainable from an economic and environmental point of view [2–5]. In the last decades, it was widely used for the remediation of groundwater contaminated by chlorinated compounds as a filling material for permeable reactive barriers (PRBs) [6–8]. Recently, ZVI was also tested for the degradation of TCE in the gas phase in view of its application in horizontal permeable reactive barriers (HPRBs), which is placed in the unsaturated zone above the source of contamination [9,10].

The degradation mechanism of chlorinated contaminants induced by ZVI is the abiotic reductive dehalogenation, in which iron is oxidized and chlorinated compounds are reduced with the progressive substitution of a chlorine atom with hydrogen [1,11–13]. The reductive dehalogenation reactions induced by ZVI occur through an electron transfer provided by iron oxidation following both hydrogenolysis and β-elimination pathways, where the latter is predominant, thus avoiding the formation of toxic byproducts, such as vinyl chloride (VC) [9].

To improve ZVI reactivity, transition metals with a redox potential higher than iron have been used as catalysts for dechlorination through the enhancement of iron corrosion or hydrogenation [2,5,12,14]. Among transition metals, the most studied as cata-

lysts for the degradation of chlorinated compounds induced by iron were palladium (Pd) [2,3,15–19], nickel (Ni) [2,15,17,18,20–26], and copper (Cu) [2,5,12,15,17,18,20]. To a lower extent, ruthenium (Ru) [3], silver (Ag) [3,15,18], cobalt (Co) [17], zinc (Zn) [27,28], and platinum (Pt) [3,17] were also tested. In general, adding these metals to iron creates a galvanic cell [15,23]. In these conditions, greater corrosion of ZVI occurs with a consequent increase in the release of electrons necessary for the reduction of chlorinated contaminants [5,29]. Furthermore, several transition metals, such as Pd or Ni, are hydrogenation catalysts [2,18,26] able to catalyze the dissociation of molecular hydrogen generated by water reduction, and thus the release of atomic hydrogen, which is useful for dechlorination reactions [2,23,29–31]. Moreover, the addition of a secondary transition metal to ZVI lowers the activation energy of the dehalogenation reaction, thus limiting the formation of oxide layers, which can reduce the electron transfer during the dechlorination process [2,23,32]. Furthermore, with the addition of these metals, it is possible to increase the degradative capacity of ZVI toward various chlorinated recalcitrant compounds, such as polychlorinated biphenyls (PCBs) or pentachlorophenol (PCP) [12,16,33].

In general, the increase in reactivity depends on the properties of the contaminants and on the choice of the catalyst metal added [34]. For instance, with the use of Cu, the prevalent mechanism that occurs is galvanic corrosion, as this metal has a positive corrosion potential [14,35,36]. In contrast, with the use of Ni, the dissociation of H_2 and hydrogenation occur predominantly. In addition, these effects are prevalent compared with the electron transfer for the enhancement of dechlorination as the presence of atomic hydrogen allows the breakage of the Cl–C bond replacing chlorine, which is released as a gas [15,24,29,35]. Indeed, Kim and Carraway, [2] and Venkateshaiah et al. [15] obtained different performances in the removal of TCE in the aqueous phase depending on the secondary metal used in combination with iron for the different effects that secondary metals induced on dechlorination, obtaining better performance using Pd and Ni compared with Cu.

In general, to obtain these catalytic phenomena, a complex formed by zero-valent iron and a secondary catalyst metal (i.e., ZVI bimetal) is created [30]. A ZVI bimetal can be synthesized through chemical or physical methods [24]. Among the chemical methods, the most commonly used is chemical solution deposition (CSD), in which a redox reaction takes place between iron and a secondary metal, where the latter is added as chloride or sulfate [2,5,36,37]. With the use of this technique, a bimetal is synthesized by spontaneous adsorption and deposition of the secondary metal on the iron particles, resulting in surface coverage of the primary metal particles [3,15,24,30,37,38]. The structure of this bimetal (i.e., core-shell) guarantees a lower oxidation of iron, which constitutes the core, due to the surface coating of the secondary metal that acts as a protection for the formation of iron oxides and as a catalyst for electrons release by the ferrous core during dehalogenation reactions [25]. In CSD, an excessive deposition of the secondary metal should be avoided as it can lead to the complete coverage of iron, thus reducing the bimetal reactivity [38]. For this reason, only bimetals with low percentages by weight of secondary metal can be synthesized by CSD [36]. Moreover, the catalyst covering the iron surface can flake off and be released in water during dechlorination, which results in a loss of the bimetal reactivity during the reactions [24,38].

These problems can be overcome using physical methods to produce bimetals, such as mechanical alloying, in which mechanochemical reactions between solid phases take place by providing energy [30,39]. The advantages of using physical techniques are short operating times, easy production, and the non-use of reagents and solutions [30,37]. Among physical methods, ball milling (BM) is widely used to produce ZVI bimetals [5,24,40–43]. In particular, the bimetal is created by inserting iron and the secondary metal powders inside a ball mill, where the continuous breaking of the particles occurs through the ball-powders collision [37]. Using BM, a bimetallic phase is obtained where catalyst particles are homogeneously distributed in the iron, rather than constituting only a surface coverage [41]. Producing this type of bimetal structure could increase the reactivity toward chlorinated

contaminants. For instance, Xu et al. [24] prepared Fe-Ni bimetals with both synthesis methods of CSD and BM to dechlorinate 4-chlorophenol (4-CP) in the aqueous phase and obtained the best performance in terms of catalytic activity and stability using the ball-milled bimetals. Therefore, BM is effective in producing bimetallic systems with high percentages of secondary metal and controllable mass fraction ratios [5].

In this study, we investigate the feasibility of using zero-valent bimetals to enhance the degradation of TCE in the gas phase, which is induced by ZVI in partially saturated conditions. To our knowledge, no similar bimetals were previously studied to treat chlorinated solvents in the gas phase. In contrast, ZVI-based bimetals can have a potential application as constituent materials for HPRBs aimed at interrupting the migration pathway of chlorinated vapors from contaminated soil and groundwater into air ambient or overlying buildings, which can cause potential risks for human health. As transition metals, we selected Ni and Cu, which as previously discussed, proved to be effective for the enhancement of the TCE degradation by ZVI in the aqueous phase [2,15,17,18,20–25]. For this purpose, different ZVI bimetals were synthesized by mixing Fe and Ni or Cu powders using the physical method of disc milling. Therefore, Fe-Cu and Fe-Ni bimetals were produced with three different percentages by weight (1%, 5%, 20%) through charging a disc mill with iron and the secondary metal powders, which allows for the production of a bimetallic phase by the continuous fracture of the particles, which is induced by the impact of the disc powders. The properties of the produced bimetals were investigated in terms of morphology, crystallographic structure, and specific surface by scanning electron microscopy equipped with energy dispersive X-ray spectroscopy (SEM-EDS) analysis, X-ray diffraction (XRD) characterization, and Brunauer–Emmett–Teller (BET) method, respectively. Furthermore, degradation tests of TCE in the gas phase with the produced bimetals at partially saturated conditions were carried out to evaluate the catalytic effect of bimetals on dechlorination reactions.

2. Materials and Methods

2.1. Materials

The iron powder used in the present work to synthesize Fe-Cu and Fe-Ni bimetals was the one already tested in a previous study by our group [10]. This material, named Fe1 in the original reference, allowed for the achievement of the best performance in terms of TCE removal in the gas phase compared with other tested iron powders. Herein, the different bimetals analyzed and tested (both supplied by Sigma-Aldrich, St. Louis, MO, USA) were produced using iron powder together with copper powder (99%, d < 75 μm) or nickel powder (99.7%, d < 50 μm). TCE (99+%), which was used in the TCE degradation tests, was supplied by Alfa Aesar (Haverhill, MA, USA).

2.2. Preparation of Fe-Cu and Fe-Ni Bimetals

In this study, two types of ZVI bimetals were prepared using iron as primary metal and Cu or Ni as secondary metal. For each bimetallic system, three different percentages of Cu or Ni were tested to assess the effect that an increasing amount of secondary metal can exert on the characteristics and TCE degradation performance of the produced materials. In particular, based on the results of previous studies performed on Fe-Cu and Fe-Ni bimetals for the degradation of chlorinated contaminants in the aqueous phase (e.g., [5,24,43]), it was decided to produce bimetals containing 1%, 5%, and 20% by weight of secondary metal (Cu or Ni). The bimetals synthesized in this work are summarized in Table 1. Each bimetal was produced by milling iron and secondary metal powders for 1 h at 700 rpm using a disc mill (*Retsch RS 200*, Retsch, Haan, Germany). The milling conditions were selected on the basis of previous studies on bimetals produced by ball milling (e.g., [39,44]) to obtain a micrometric material. As reference, the same milling treatment was also applied to the iron powder alone to evaluate the possible effect on the morphology and particle dimension of this material. Furthermore, mixtures of iron powder with 5% Cu or 5% Ni without milling (named in this study Fe-5%Cu* and Fe-5%Ni*) were also prepared to characterize them and

compare their properties with those of the milled mixtures (i.e., ZVI bimetals) containing the same amount of secondary metal (see Table 1). In addition, to evaluate if a shorter milling time could still ensure the formation of a bimetal, the Fe-5%Ni mixture was milled for 10 and 30 min at 700 rpm.

Table 1. Produced materials, specific surface area (SSA) values quantified, and percentage composition estimated by scanning electron microscopy with energy dispersive X-ray spectroscopy (SEM-EDS).

Material	Treatment	SSA (m^2/g)	Fe (%)	Cu (%)	Ni (%)
Cu	-	0.5	-	-	-
Ni	-	0.5	-	-	-
Fe	Milling	0.3	-	-	-
Fe-1%Cu	Milling	0.7	98.4	1.6	-
Fe-5%Cu	Milling	<LOQ	95.3	4.7	-
Fe-20%Cu	Milling	0.5	81.9	18.1	-
Fe-1%Ni	Milling	0.3	99.0	-	1.0
Fe-5%Ni	Milling	0.3	94.8	-	5.2
Fe-20%Ni	Milling	0.2	85.3	-	14.7
Fe-5%Cu*	-	-	97.4	2.6	-
Fe-5%Ni*	-	-	89.1	-	10.9

2.3. Materials Characterization

The Cu and Ni powders, the milled iron powder, and the bimetallic materials produced were characterized to analyze their morphology, crystallographic structure, and specific surface area (SSA). The morphology of the samples, in terms of particles dimension, elemental composition, and mapping, was analyzed by scanning electron microscopy (SEM) (*FE-SEM, SUPRA™ 35, Carl Zeiss SMT*) equipped with energy dispersive X-ray spectroscopy (EDS). Namely, for each material produced, the SEM-EDS analysis allowed for the assessment of the elemental composition of the produced materials, as well as the evaluation of the spatial distribution of the secondary metal in the particles of the obtained bimetal. As reference, the same analysis was also carried out on the two mixtures that were not subjected to the milling treatment. The crystallographic structure of the tested materials was investigated by X-ray diffraction (XRD) analysis: θ–2θ scans in the range of 40–85° were performed on *Rigaku Diffractometer* in the Bragg Brentano configuration using Cu Kα radiation. The diffraction peaks in the patterns were compared with ICSD database. The specific surface area (SSA) of the samples was evaluated by the Brunauer–Emmett– Teller (BET) method using N$_2$ adsorption at 77 K with a *Micromeritics ASAP2020* apparatus. SSA (m^2/g) values were calculated in accordance with a previous study [45].

2.4. TCE Removal Experiments

Batch degradation tests were performed using the experimental setup already adopted by Zingaretti et al. [9,10], in view of the application of the produced bimetals for the degradation of TCE in the gas phase. All the materials used in the TCE degradation tests were pretreated by maintaining them in contact with 0.1 M HCl for 1 h and then washing them with ultrapure (UP) water previously fluxed with N$_2$, following the procedure reported by Zingaretti et al. [10]. Acid washing allows for the removal of oxide layers on the particles of iron, which may have formed from reactions with the oxygen present in the air to which the material is exposed [37] and also allows for an increase in the reactivity toward dechlorination [9]. Furthermore, acid washing of the Fe-Ni bimetals increases the generation of hydrogen on the surface of the particles [46], which is useful in the dehalogenation reactions. Following the pretreatment, each material was dried at anaerobic conditions by flushing a nitrogen flow directly on the washed material and then conserved in N$_2$ atmosphere to prevent the formation of oxide layers.

The TCE degradation tests were carried out at room temperature in transparent glass vials (20 mL) and were prepared by adding 1 g of reactive material (milled iron

or bimetal), after purging the vial with N_2 to promote anaerobic conditions. UP water (100 μL), previously flushed with N_2, was added to the reactive material to obtain a water content of 10% by weight [9,10]. The addition of water is necessary as it constitutes a proton donor, which is necessary for TCE degradation reactions induced by zero-valent iron [1] and catalyzed by adding Cu or Ni [2]. Subsequently, TCE (5 μL) was injected into a glass tube (1 mL), from which it could volatilize, and finally the vials were closed with aluminum caps equipped with PTFE-faced silicone septa. In addition to the degradation tests, control tests without adding the reactive material were carried out. Degradation and control tests were carried out in parallel to assess the potential TCE losses from the vial. For each produced material, a reaction time of 1 day was tested.

The residual TCE concentration at the end of the test was quantified in the headspace of the vials by gas chromatography with a flame ionization detector (GC-FID). In particular, 250 μL of TCE gas were sampled from the vial's headspace and injected by an automatic sampler (*PAL System*, *AOC-5000plus*), with a split ratio of 1:10, to a gas chromatograph (*Shimadzu GC, GC_QP2010SE*) equipped with an Equity 5 column (30 m × 0.25 mm ID × 0.25 μm film thickness). The carrier gas used was Helium with a flow rate of 0.9 mL/min. The oven temperature ramp was programmed to start from 40 °C, remained for 2 min, with an increase of 8 °C per minute to 150 °C, that remained for an additional 2 min.

3. Results and Discussion

3.1. Microstructure and Morphology

In Figure 1, the morphologies of milled iron, copper and nickel powders are illustrated. The Fe sample (Figure 1a) is characterized by micrometric particles with a heterogeneous size distribution estimated in the range of 2–30 μm. The surface of Fe particles appears to be relatively smooth, possibly due to the disc milling treatment. The Cu sample (Figure 1b) is characterized by micrometric particles with dimensions lower than 75 μm, in accordance with the manufacturer's information. Cu particles resemble agglomerates of rounded and tapered formations. The Ni sample (Figure 1c) has a homogeneous size distribution of micrometric particles in the dimensional range of 10–30 μm and shows a stratified morphology, which is created by formations similar to overlayed triangular gills.
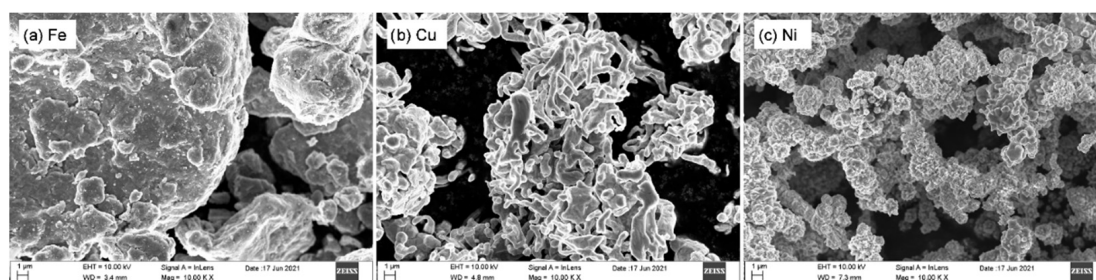

Figure 1. SEM images of the base materials: Milled iron powder (**a**), copper powder (**b**), nickel powder (**c**).

In Figures 2 and 3, the morphologies of the different types of Fe-Cu and Fe-Ni bimetals produced are shown. For each sample analyzed, two images at different magnifications are shown. The image at lower magnification reveals an overview of the particles produced and is compared to evaluate their dimensional homogeneity and average size. In contrast, the image at higher magnification reveals the details of the single particle and is compared to evaluate whether there is evidence of the secondary metal particles on the surface. The morphology of Fe-Cu bimetals appears to be similar to the milled iron powder, which is possibly due to the same milling treatment. From the reported images (Figure 2a,c,e), it is possible to observe that by increasing the Cu content in the bimetal, larger particles are obtained with an increasing irregular particle size distribution. Namely, the Fe-1%Cu sample is characterized by a rather homogeneous particle size distribution in the range of 5–60 μm (Figure 2a) with a relatively smooth surface (Figure 2b). In contrast, the Fe-5%Cu

sample is characterized by a larger and less homogeneous particle size distribution in the range of 30–100 µm (Figure 2c) and a less smooth surface (Figure 2d). Meanwhile, the Fe-20%Cu sample has an irregular size distribution of particles in the range of 20–50 µm, with the presence of agglomerated particles reaching a size of 150 µm (Figure 2e). In addition, the sample is characterized by a rough surface, in which some formations, similar to residual copper particles, are observed on the surface of the particles (Figure 2f).
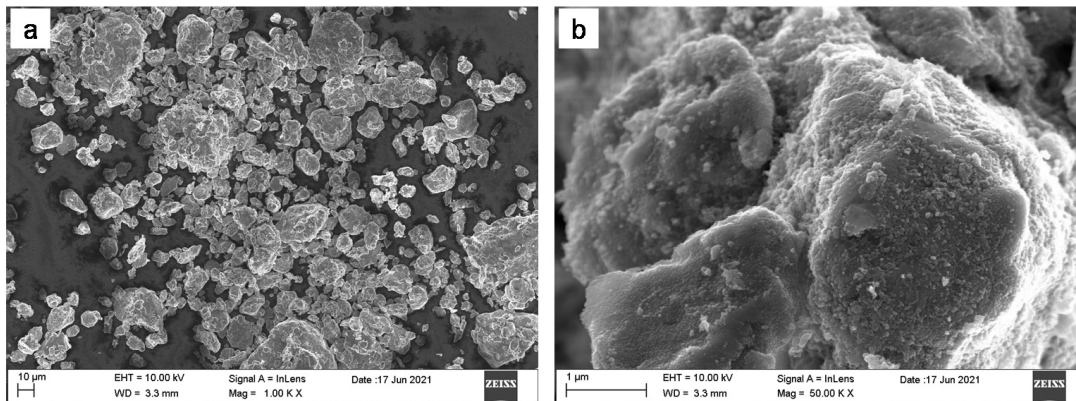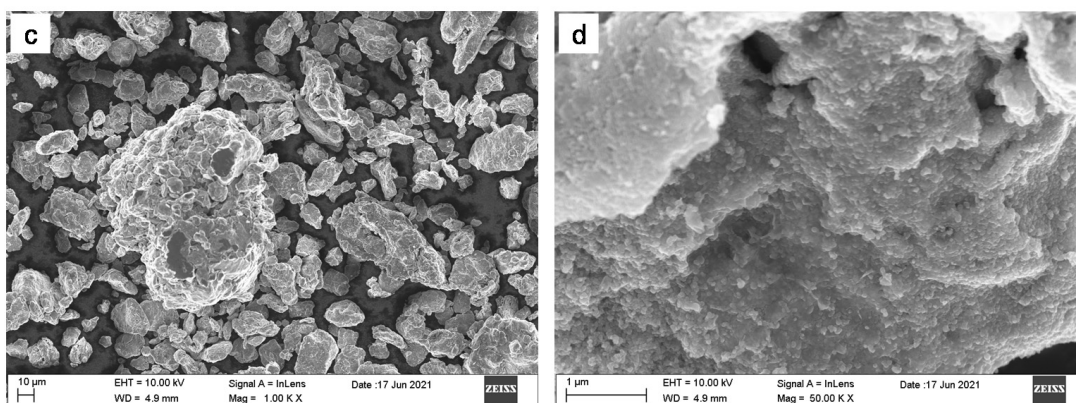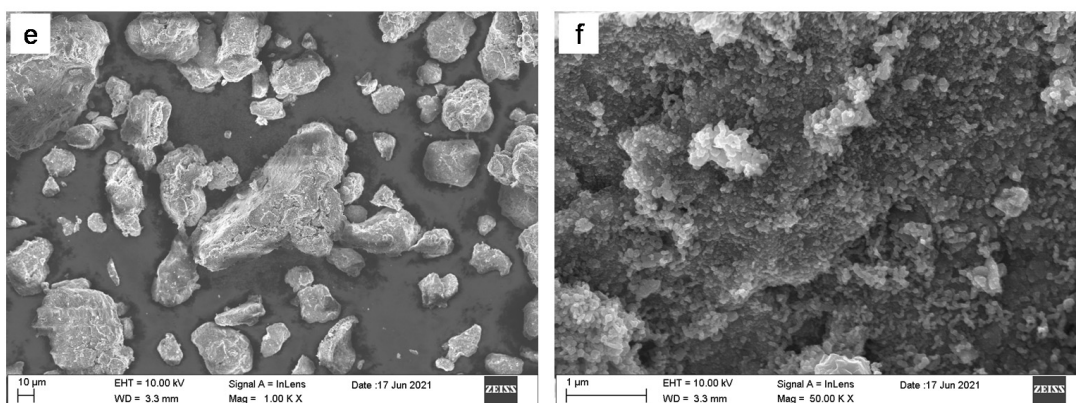

Figure 2. SEM images of Fe-Cu bimetals: Fe-1%Cu (**a**,**b**), Fe-5%Cu (**c**,**d**), Fe-20%Cu (**e**,**f**).

Bimetal Fe-1%Ni

Bimetal Fe-5%Ni
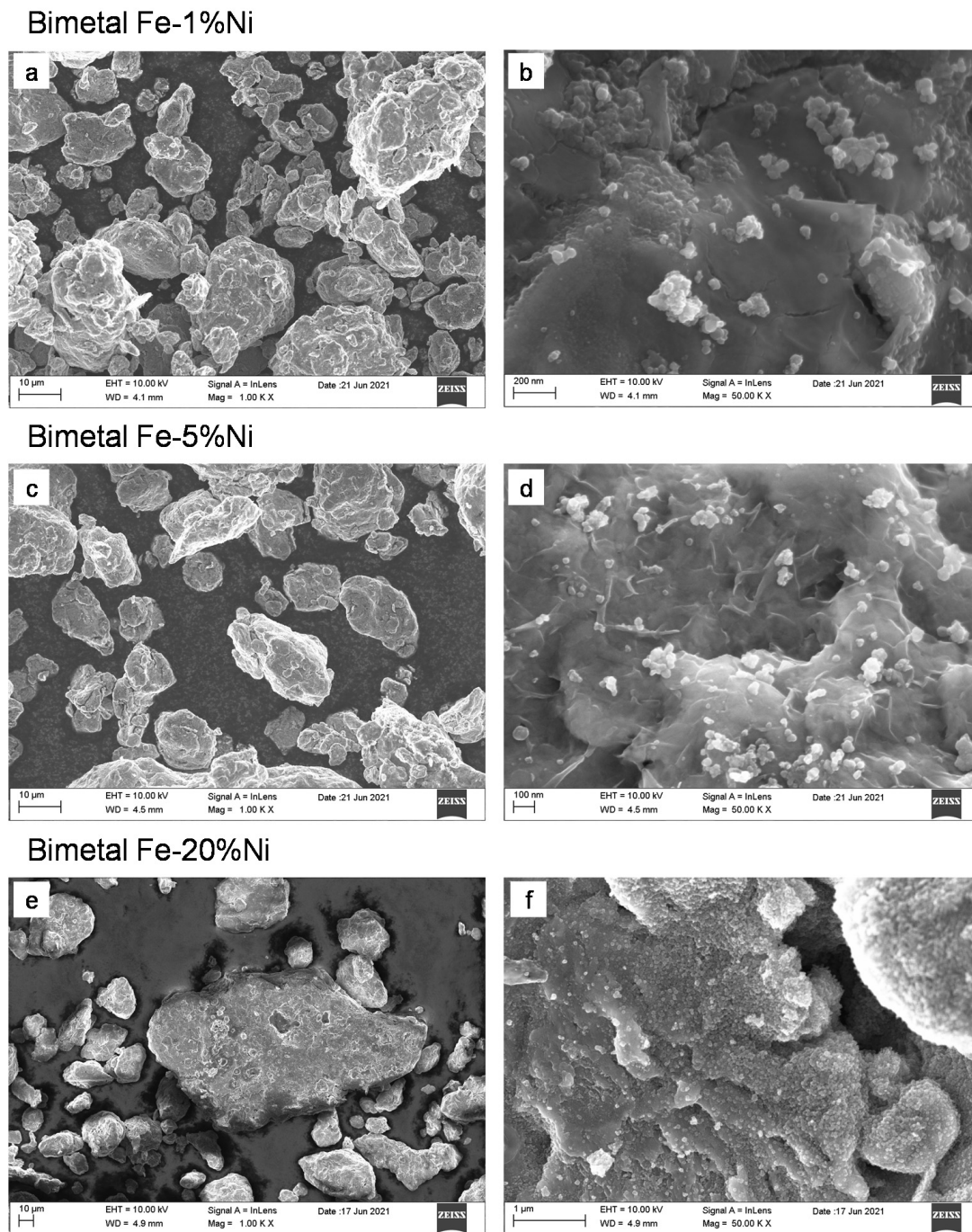
Bimetal Fe-20%Ni

Figure 3. SEM images of Fe-Ni bimetals: Fe-1%Ni (**a**,**b**), Fe-5%Ni (**c**,**d**), Fe-20%Ni (**e**,**f**).

The morphology of Fe-Ni bimetals reported in Figure 3 appears to be similar to the milled iron powder and Fe-Cu bimetals. Moreover, in this case, by increasing the Ni content, larger particles are obtained and the surface of the particles appears to be rougher with the presence of formations, which is possibly related to nickel as a separate phase. The Fe-1%Ni sample is characterized by a rather homogeneous particle size distribution in the range of 5–60 μm (Figure 3a) with a relatively smooth surface (Figure 3b). The Fe-5%Ni sample is characterized by a larger and relatively homogeneous particle size distribution in the range of 20–90 μm (Figure 3c) with a flaked smooth surface (Figure 3d). Meanwhile, the Fe-20%Ni sample shows an irregular size distribution of particles (from 10 to 100 μm) (Figure 3e) and a lumpy surface with nickel residual formations (Figure 3f). The surfaces of the particles of

the bimetals produced are also reported in Figure S1 at a high value of magnification to better appreciate the differences among the different materials described above.

Note that the resolution of the SEM instrument adopted in this study (*FE-SEM, SUPRA™ 35, Carl Zeiss SMT*) is in the order of 1–2 nm. Therefore, the presence of particles characterized by a lower size cannot be detected with this type of analysis.

3.2. Elemental Mapping

In Figures 4 and 5, the SEM-EDS images and mapping of Fe-Cu and Fe-Ni bimetals are shown. The SEM-EDS analysis was carried out on samples taken from a lab-scale grinding (i.e., 20 g). In Fe-1%Cu (Figure 4c), Fe-5%Cu (Figure 4f), and Fe-20%Cu (Figure 4i), it is possible to notice that Cu (red dots) is homogeneously dispersed in the iron phase with a rising concentration as the dosage of copper was increased. Similar results were observed for Fe-Ni bimetals in Figure 5c,f,i for Fe-1%Ni, Fe-5%Ni, and Fe-20%Ni. Homogeneity of Fe-Cu bimetallic systems, which is synthesized by milling, was also observed in previous studies (e.g., [5,41,47]). Furthermore, homogeneous Ni dispersed in the iron phase in Fe-Ni bimetals, which is produced by milling, was noticed in other works (e.g., [24,38]).
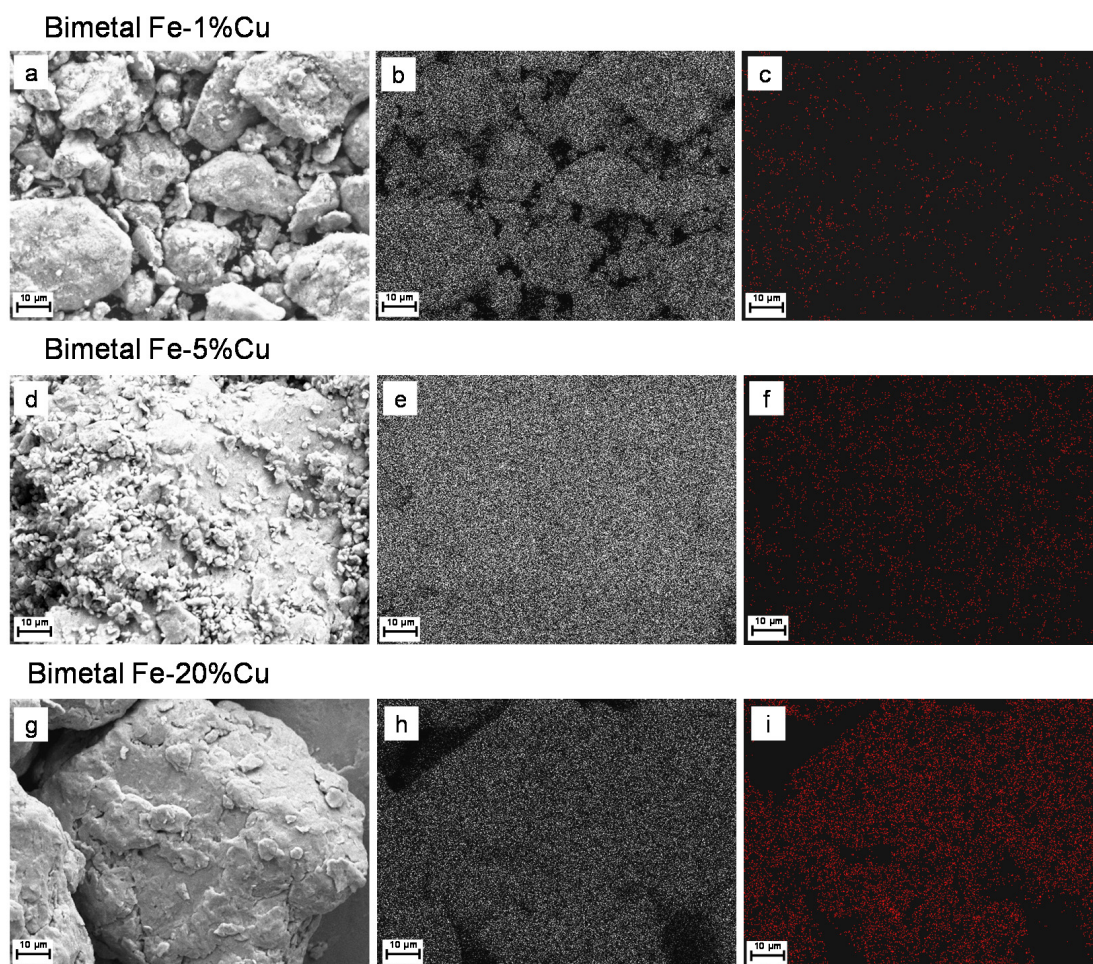

Figure 4. Elemental mapping of Fe-Cu bimetals: SEM-EDS images (**a**,**d**,**g**), Fe maps (**b**,**e**,**h**), and Cu maps (**c**,**f**,**i**).

The elemental composition of the Fe-Cu and Fe-Ni bimetals produced was also quantified by EDS and the obtained results are reported in Table 1. The weight percentages estimated are very close to the theoretical values of 1%, 5%, and 20%. This constitutes the homogeneity in composition of the synthesized bimetallic particles. As reference, Figure 6 shows the SEM-EDS images for the unmilled Fe-5%Cu and Fe-5%Ni mixtures, named Fe-5%Cu* and Fe-5%Ni*, respectively in this work. In this case, it is possible to clearly

distinguish Fe and Cu (Figures 6a and S2a,b) or Ni (Figures 6d and S2c,d) morphologies. In addition, EDS indicates a heterogeneous distribution of the secondary metals on the iron phase (Figure 6c,f). These results point out that mixing the two metal powders is not sufficient to synthesize a bimetal, which is also shown by Liu et al. [5] and Xu et al. [24]. Furthermore, the weight percentages estimated by EDS for the Fe-Cu and Fe-Ni mixtures are not consistent with the theoretical composition, further indicating that no bimetal was produced (see Table 1).
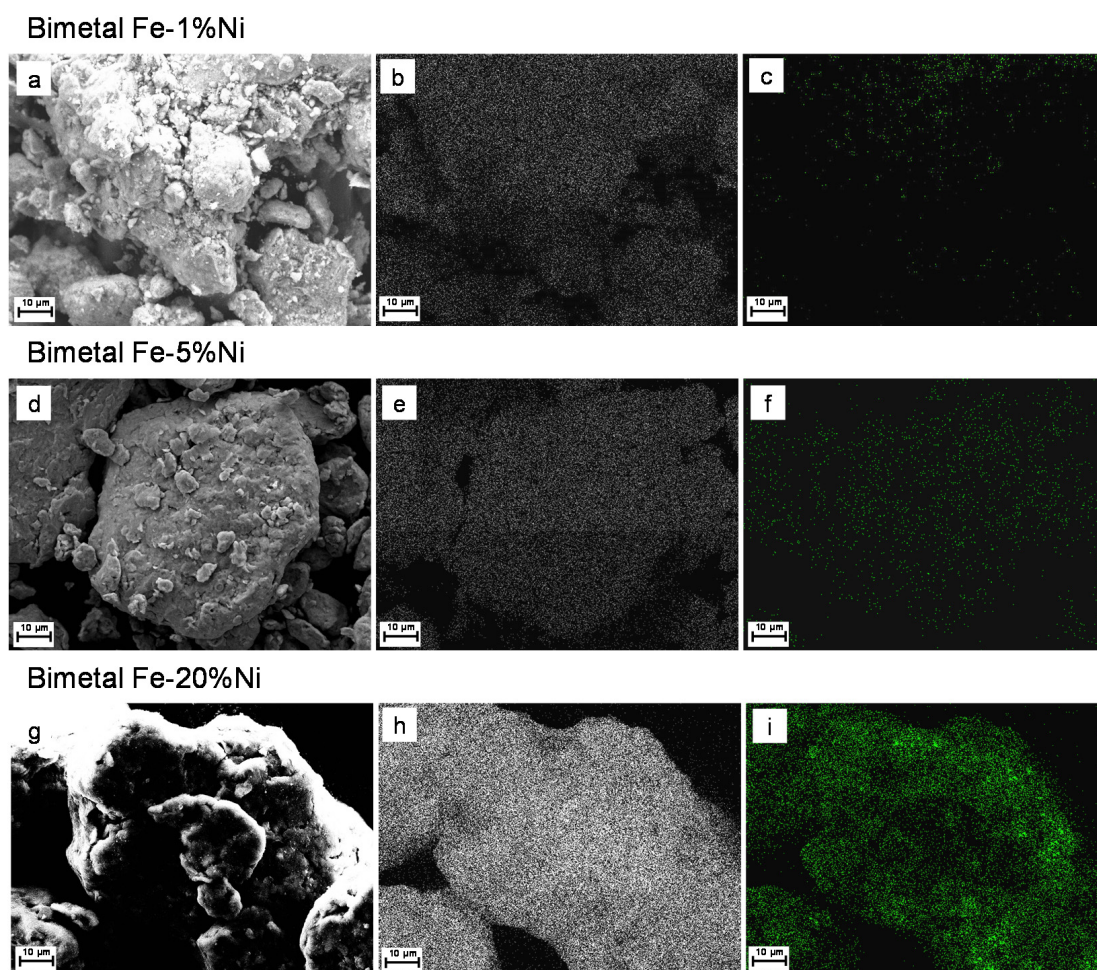

Figure 5. Elemental mapping of Fe-Ni bimetals: SEM-EDS images (**a**,**d**,**g**), Fe maps (**b**,**e**,**h**), and Ni maps (**c**,**f**,**i**).

3.3. XRD Characterization

The XRD patterns of the bimetals Fe-1%Cu, Fe-5%Cu, Fe-20%Cu and of milled iron and Cu are shown in Figure 7a,b, whereas those of the bimetals Fe-1%Ni, Fe-5%Ni, Fe-20%Ni and of milled iron and Ni are shown in Figure 7c,d. In the disc milled iron, copper and nickel samples, the only crystalline phases detected by XRD are related to metallic Fe, Cu or Ni, respectively, without macro impurities (see Figure 7a,c). However, the presence of trace elements (in the order of, e.g., mg/kg) could not be excluded for the limits of quantification of XRD analysis.

For the Fe-Cu and Fe-Ni bimetals, with a Cu content of 1–5% and a Ni content of 1–5%, respectively, the central cubic phase of the body (bcc) typical of the iron crystal, persists due to the formation of the bimetallic phase. Furthermore, it is possible to notice that in the diffraction pattern the Cu (200), Cu (220), Ni (200), and Ni (220) peaks are almost completely absent, as copper and nickel were possibly involved in the formation of the Fe-Ni and Fe-Cu bimetallic phase (see Figure 7, blue and red lines, respectively). For the

samples Fe-20%Cu and Fe-20%Ni, the presence of the Cu (111), Cu (200), and Ni (200) peaks in the diffraction patterns indicates the existence of small amounts of Cu and Ni as segregates, which is not included in the bimetallic phase in both compositions (Figure 7a,c, green line). These aspects are confirmed from SEM analysis (see Figures 2f and 3f). For all the Fe-Cu samples examined, the (110) peak position remains constant for the different concentrations of Cu present in the bimetallic phase (Figure 7b). The lattice parameter of the bimetallic phase, calculated from the peak (110), results in value of a = 2.86 Å and does not change significantly with the Cu content [48].
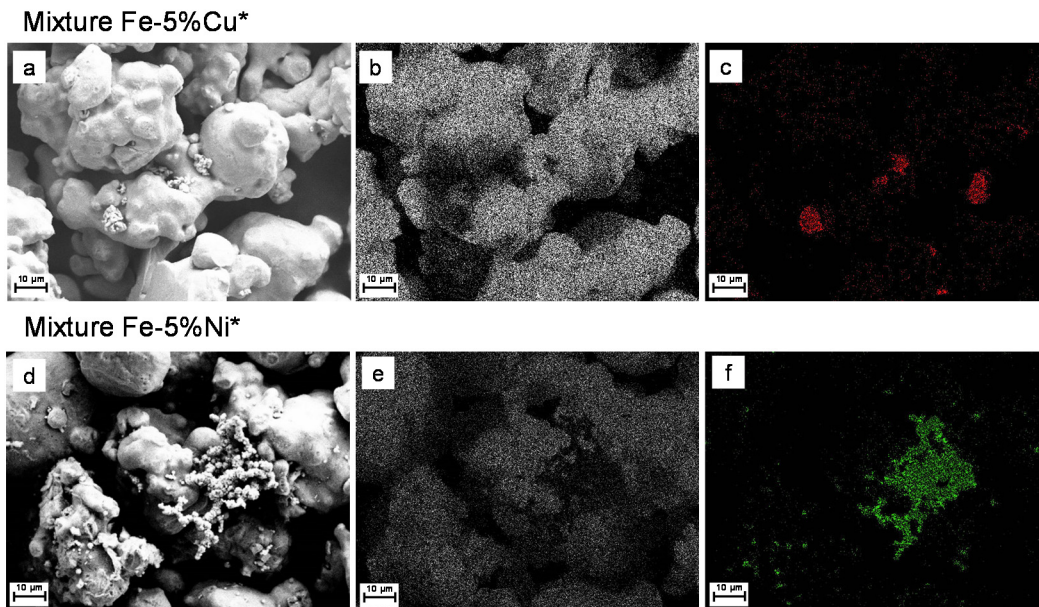

Figure 6. Elemental mapping of Fe-5%Cu* and Fe-5%Ni* mixtures: SEM-EDS images (**a**,**d**), Fe maps (**b**,**e**), Cu map (**c**), and Ni map (**f**).
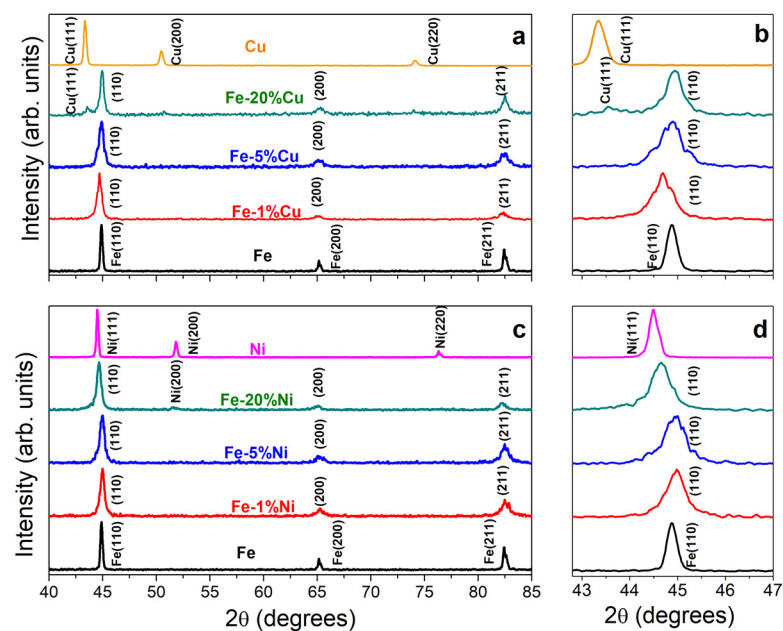

Figure 7. XRD θ–2θ patterns for Fe-Cu and Fe-Ni bimetals: (**a**) Fe-1%Cu (red line), Fe-5%Cu (blue line), Fe-20%Cu (green line), Fe (black line), and Cu (yellow line) in the range of 40–85° and (**b**) 43–47°; (**c**) Fe-1%Ni (red line), Fe-5%Ni (blue line), Fe-20%Ni (green line), Fe (black line), and Ni (purple line) in the range of 40–85° and (**d**) 43–47°.

On the other hand, for the Fe-Ni bimetallic phase, a progressive displacement of the (110) peak to a lower 2θ angle is observed as the Ni quantity increases (Figure 7d). These different trends for Fe-Cu and Fe-Ni are possibly due to the different ionic radius of the component elements, which can have an effect on the internal strain of the grains [24,49,50]. In Figure 8, the diffraction patterns of the bimetal Fe-5%Ni milled for 0, 10, 30, and 60 min as compared with the milled iron and Ni are shown. For the unmilled sample (0 min), the diffraction pattern shows the separate presence of the Ni (111) and Fe (110) peaks in the range of 44.2–45.2°, thus suggesting that the Fe-Ni bimetal formation did not occur (Figure 8b). Conversely, for samples milled for 10, 30, and 60 min, only the peaks attributed to the Fe-Ni bimetallic phase are present and the reflections Ni (200) and Ni (220) are no longer present. This behavior is in agreement with the literature [49]. The lattice parameter calculated for all samples remains constant (a = 2.86 Å).
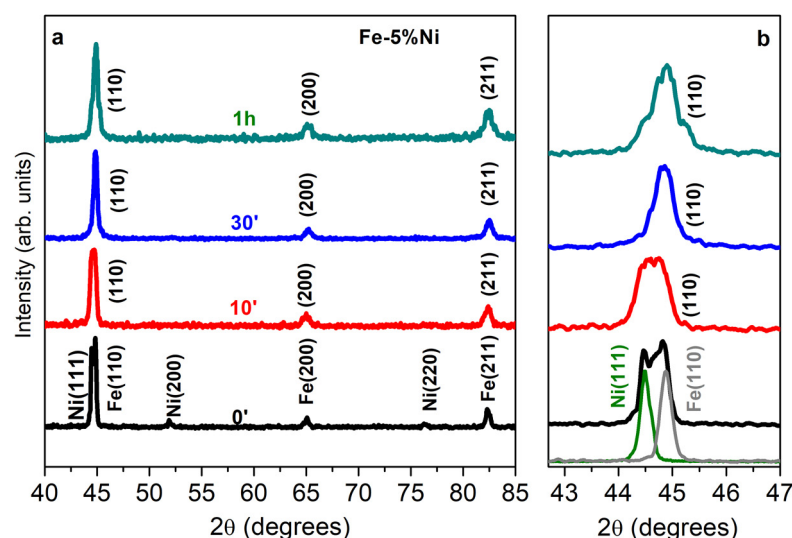

Figure 8. XRD θ–2θ patterns for Fe-5%Ni: Unmilled (black line), milled for 10 min (red line), 30 min (blue line), and 60 min (green line) in the range of 40–85° (**a**) and 43–47° (**b**). Ni (dark green line) and Fe (grey line) (**b**).

3.4. Specific Surface Area

Table 1 reports the SSA (m^2/g) values obtained for milled iron, copper, and nickel powders and for Fe-Cu and Fe-Ni bimetals produced. The profiles of adsorption–desorption isotherms of the samples were of Type II of International Union of Pure and Applied Chemistry (IUPAC) classification [51] without hysteresis, which is characteristic of non-porous materials (Figure S3). The SSA values quantified for the samples analyzed are in the range of 0.2–0.7 m^2/g, except for the Fe-5%Cu bimetal, for which the specific surface area resulted in a lower value than the quantification limit (LOQ). The values obtained are in line with previous studies. For instance, Xu et al. [24] produced a ball-milled Fe-15%Ni bimetal and obtained a specific surface area of 0.49 m^2/g.

3.5. TCE Removal Using Different Fe-Cu and Fe-Ni Bimetals

In Figure 9, the results of TCE degradation tests using the different bimetals produced for a reaction time of 1 day are shown. The results achieved using the milled iron powder are also reported as reference. It can be observed that the milled iron powder alone led to a TCE degradation in the gas phase of around 44%. For Fe-Cu bimetallic systems, the best removal performance of around 57% was obtained using the bimetal with the lower Cu content, while by increasing this value, TCE removals of around 41–46% were observed, similar to the results obtained using the disc milled iron. On the other hand, better results were achieved using Fe-Ni bimetals. Namely, adding the Ni content of 1%, it was possible to enhance the reactivity of iron by removing 55% of TCE in the gas phase. Furthermore, by

increasing the Ni content to 5%, the best result in terms of TCE degradation was obtained (75% of removal) and the performance remained constant using the bimetal with 20% of Ni (73% of removal). Therefore, higher TCE removals than Fe alone were obtained using the Fe-Ni (1%, 5%, 20%) bimetals or the Fe-Cu bimetals, but were limited to the lowest Cu content (1%).
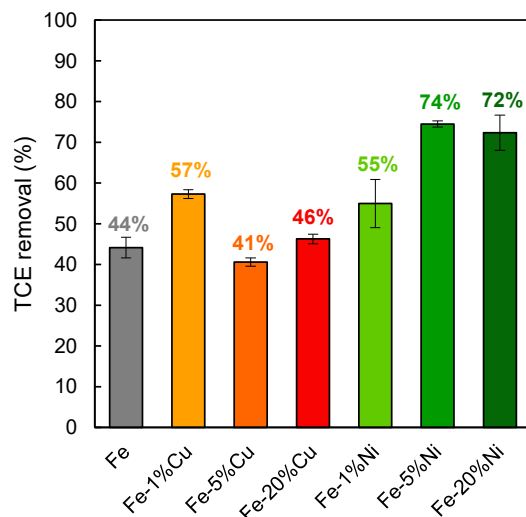

Figure 9. TCE removal at 1 day of reaction time using milled iron and bimetals.

These results are consistent with previous studies carried out on the aqueous phase. For instance, Liu et al. [5] studied the degradation of 4-CP in the aqueous phase by ball-milled Fe-Cu bimetals and noticed that the dechlorination activity was reduced when the copper content increased. On the other hand, other studies highlighted that nickel has a better catalytic activity toward dechlorination than copper [52]. For example, Kim and Carraway, [2] and Venkateshaiah et al. [15] produced various bimetallic systems through the chemical deposition technique for the degradation of TCE in aqueous phase and obtained a better reactivity of Fe-Ni bimetals compared with Fe-Cu. In addition, Xu et al. [24] noticed an enhanced reactivity toward dehalogenation of 4-CP in the aqueous phase, which increases the Ni content in ball-milled Fe-Ni bimetals. In this study, by considering that the SSA values obtained for the bimetals produced were relatively similar among the different tested materials, it can be argued that the catalysis of the dechlorination reactions induced by Cu or Ni was possibly the main factor affecting the degradation of TCE in the gas phase.

3.6. TCE Degradation Pathway, Byproducts, and Mechanism

The chromatograms obtained from the TCE degradation tests carried out with 1 day of reaction using Fe-Cu and Fe-Ni bimetals are shown in Figure 10. As reference, the chromatograms obtained at the same time of reaction using disc milled iron (Fe) and without the addition of reactive material (i.e., control tests) are also reported. In the chromatogram relative to the control test, only the TCE peak was present, i.e., no degradation products were detected. In contrast, the addition of a reactive material led to TCE degradation with a consequent formation of various reaction byproducts. Specifically, using disc milled iron and Fe-Cu or Fe-Ni bimetals, the same degradation products were found with various intensities depending on the TCE degradation capacity of the different bimetals tested. In general, the intensity of the peaks of the byproducts is directly related to TCE degradation. In fact, higher peaks of dechlorination products were found in the chromatograms obtained in the tests performed with Fe-Ni bimetals (see Figure 10b) compared with those detected in the Fe-Cu tests (see Figure 10a) due to the better catalytic ability of Ni compared with Cu (see Figure 9). The degradation products observed in this study are similar to those found and identified by Zingaretti et al. [9,10] in degradation tests of TCE in the gas phase, which

are carried out using different types of zero-valent iron. In particular, these byproducts were identified as C_{3-6} hydrocarbons.
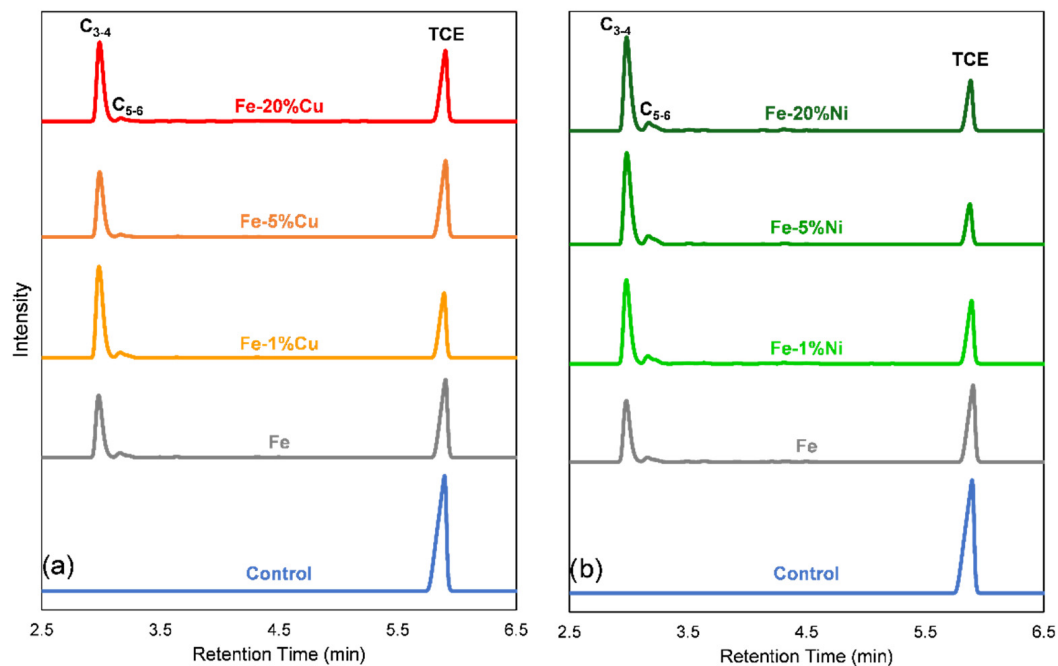

Figure 10. Gas chromatography with flame-ionization detection (GC-FID) chromatograms obtained in TCE degradation tests with Fe-Cu (**a**) and Fe-Ni bimetals (**b**). TCE degradation test using Fe and control tests are also reported as reference.

Based on these results, for each degradation test, a mass balance comparing the residual TCE ($M_{residual.TCE}$) and byproducts ($M_{degraded.TCE}$), which are detected at the end of the experiment with the mass of TCE and measured in the control test ($M_{control.TCE}$), was performed:

$$TCE\ Mass\ Balance\ (\%) = \left(\frac{M_{residual.TCE}}{M_{control.TCE}} + \frac{M_{degraded.TCE}}{M_{control.TCE}} \right) \cdot 100 \tag{1}$$

with:

$$\frac{M_{residual.TCE}}{M_{control.TCE}} = \frac{A_{residual.TCE}/RF_{TCE}}{A_{control.TCE}/RF_{TCE}} = \frac{A_{residual.TCE}}{A_{control.TCE}} \tag{2}$$

$$\frac{M_{degraded.TCE}}{M_{control.TCE}} = \frac{\Sigma \left(A_{byproducts}/RF_{CnHm} \cdot \gamma_{TCE/CnHm} \right)}{A_{control.TCE}/RF_{TCE}} \tag{3}$$

where $A_{residual.TCE}$, $A_{byproducts}$, and $A_{control.TCE}$ are the areas of the chromatograms obtained at the end of each test (see Figure 10) for the residual TCE, the C_{3-6} hydrocarbon byproducts, and the TCE in the control test, respectively; RF_{TCE} and RF_{CnHm} are the GC-FID response factors of TCE and C_{3-6} hydrocarbons; and $\gamma_{TCE/CnHm}$ is the stoichiometric mass ratio between TCE and the relative byproducts.

The stoichiometric mass ratio between TCE and the C_nH_m byproducts ($\gamma_{TCE/CnHm}$) was estimated using the following reaction:

$$nC_2HCl_3 + (2m-n)H^+ + 3ne^- \rightarrow 2C_nH_m + 3nCl^- \tag{4}$$
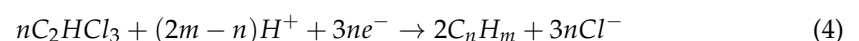
Considering the C_{3-6} hydrocarbon byproducts previously found by *Zingaretti* et al. [10] from Equation (4), an average stoichiometric mass coefficient of 4.6 g_{TCE}/gC_nH_m was obtained. Regarding the GC-FID response factor of hydrocarbons (RF_{CnHm}), the specific calibration

for C_3-C_6 hydrocarbons was not performed, rather it was introduced as a relative response factor between TCE and C_3-C_6 hydrocarbons ($RRF_{CnHm/TCE}$) and expressed as:

$$RRF_{CnHm/TCE} = \frac{RF_{CnHm}}{RF_{TCE}} \tag{5}$$

$RF_{CnHm/TCE}$ was assumed as equal to 5 in accordance with the average values reported in the literature for C_3-C_6 hydrocarbons [53].

Therefore, by substituting Equations (2)–(5) in Equation (1), the TCE mass balance for each degradation test was carried out as follows:

$$TCE\ Mass\ Balance\ (\%) = \left(\frac{A_{residual.TCE}}{A_{control.TCE}} + \frac{\Sigma \left(A_{byproducts} \cdot \frac{\gamma_{TCE/CnHm}}{RRF_{CnHm/TCE}} \right)}{A_{control.TCE}} \right) \cdot 100 \tag{6}$$

The outcome of the mass balance is shown in Figure 11. It can be noticed that in all of the tests, the mass balance resulted in a value almost equal to 100%, thus highlighting that the mass of the residual and degraded TCE was approximately equal to the mass of TCE detected in the control test. Therefore, it can be concluded that the removal of TCE in the gas phase, which is obtained in the different tests, can be mainly ascribed to a reduction of TCE to C_{3-6}, while other effects (e.g., adsorption of TCE on the reactive material) can be considered negligible.
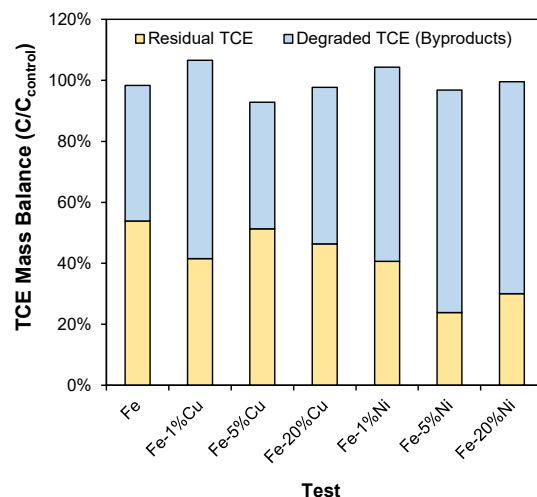

Figure 11. TCE mass balance after the degradation tests using Fe and bimetals results.

Furthermore, based on the degradation byproducts detected in the tests, it can be assumed that the main degradation pathway of TCE in the gas phase was β-elimination [9,10,54]. From the obtained chromatograms, it is also possible to observe that both disc milled iron and bimetals induced TCE dechlorination via β-elimination, thus suggesting that the addition of a secondary metal does not influence the degradation pathway of TCE, but only catalyzes the reactions. The possible mechanism of TCE removal in the gas phase induced by Fe-Cu and Fe-Ni bimetals is schematized in Figure 12. In particular, the electron transfer occurs through the Fe-Ni or Fe-Cu bimetallic particle, releasing the electrons necessary for TCE reduction. In addition, this phenomenon is accelerated by the presence of Cu or Ni [5,24]. Furthermore, in the Fe-Ni bimetallic particle, the dissociation of H_2 is catalyzed and this phenomenon occurs predominantly, releasing the atomic hydrogen useful for TCE degradation [2,16]. The catalysis of electron transfer and the dissociation of molecular hydrogen induced by secondary metals enhance the transformation of TCE in C_{3-6} hydrocarbons through β-elimination pathway. To a major extent, the increase in the degradation rates occurs for Fe-Ni bimetals, where both effects take place [2].
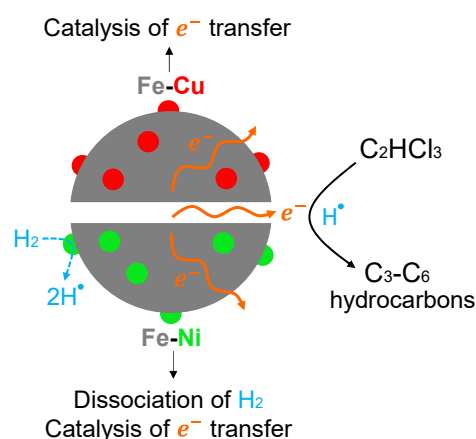
Figure 12. TCE degradation mechanism and pathway induced by Fe-Cu and Fe-Ni bimetallic particles.

4. Conclusions

The suitability of ZVI-based bimetals for the degradation of TCE in the gas phase was investigated. Different Fe-Cu and Fe-Ni bimetals with 1%, 5%, and 20% of secondary metal were produced by disc milling and characterized. SEM analysis showed that the produced bimetals presented particles in the range of micrometers. This result is important from the perspective of the potential application of ZVI-based bimetals in HPRBs to avoid problems of particle aggregation and vapor diffusion during the treatment of chlorinated compounds in the gas phase [10].

In line with other literature studies, SEM analysis [5,24] and XRD characterization [42,48] showed that in bimetals with low percentages of Cu or Ni, i.e., 1% and 5%, the secondary metal was entirely incorporated in Fe particles forming a bimetallic phase. In contrast, in bimetals with 20% of Cu or Ni, a small amount of secondary metal was observed on the surface of the produced material as a residual phase. EDS analysis showed a homogenous distribution of Cu and Ni particles in Fe phase in the bimetals produced, in accordance with previous studies [5,24]. The homogeneity of bimetals is fundamental for the enhancement of the reactivity toward dehalogenation reactions of chlorinated compounds, due to the effective and close contact between Fe and the catalyst metal [5,24,25].

Based on the results of TCE vapors degradation tests, it was possible to observe an enhancement in the dechlorination obtained using the produced bimetals compared with the corresponding milled iron powder. In particular, a TCE removal of around 57% was achieved using Fe-1%Cu bimetal, while a lower TCE removal was obtained by increasing the Cu content, in line with other literature studies carried out on the dechlorination of chlorinated compounds in aqueous phase [5,12]. In contrast, with the use of Fe-Ni bimetals, an increased reactivity toward dechlorination was noticed compared with Fe-Cu. Namely, a TCE removal in the gas phase of around 55% was achieved by adding the Ni content of 1%, whereas increasing the Ni content in the bimetals allowed for the removal of 75% of TCE vapors. The SSA values quantified for the bimetals produced were relatively similar among the different tested bimetals, thus suggesting that the enhancement in reactivity toward dechlorination of bimetals could be due to the catalysis via iron corrosion and hydrogenation. Furthermore, from the chromatographic analysis, C_{3-6} hydrocarbons were found as byproducts and it was suggested that β-elimination was the predominant degradation pathway using disc milled iron or bimetals in TCE degradation tests.

Based on the obtained results, the adoption of disc milling allows for the attainment of relatively short grinding time bimetals with homogeneous Cu or Ni dispersed in the iron phase and good reactivity toward dechlorination. In addition, the ZVI bimetals produced by disc milling proved to be effective in the treatment of TCE in the gas phase and presented characteristics that make them suitable for potential use as constituent materials for HPRBs. In the future, further degradation tests at different reaction times could be carried out to estimate the degradation kinetics of TCE in the gas phase induced by ZVI-based bimetals,

which is required for the design of horizontal permeable reactive barriers. Furthermore, to assess the longevity of these materials, specific tests could be carried out to evaluate the long-term performance of the produced bimetals.

References

1. ITRC. *Permeable Reactive Barrier: Technology Update*; Interstate Technology and Regulatory Council, PRB: Technology Update Team: Washington, DC, USA, 2011. Available online: http://www.itrcweb.org (accessed on 15 May 2022).
2. Kim, Y.H.; Carraway, E.R. Reductive dechlorination of TCE by zero valent bimetals. *Environ. Technol.* **2003**, *24*, 69–75. [CrossRef] [PubMed]
3. Lin, C.J.; Lo, S.L.; Liou, Y.H. Dechlorination of trichloroethylene in aqueous solution by noble metal-modified iron. *J. Hazard. Mater.* **2004**, *116*, 219–228. [CrossRef] [PubMed]
4. Sun, L.; Song, H.; Li, Q.; Li, A. Fe/Cu bimetallic catalysis for reductive degradation of nitrobenzene under oxic conditions. *Chem. Eng. J.* **2016**, *283*, 366–374. [CrossRef]
5. Liu, J.; Zhu, H.; Xu, F.; Zhao, J. Enhanced hydrodechlorination of 4-chlorophenol by Cu/Fe bimetallic system via ball-milling. *Desalin. Water Treat.* **2017**, *64*, 157–164. [CrossRef]
6. McCarty, P.L. Groundwater contamination by chlorinated solvents: History, remediation technologies and strategies. In *In Situ Remediation of Chlorinated Solvent Plumes*; Springer: New York, NY, USA, 2010; pp. 1–28.
7. Phillips, D.H.; Nooten, T.V.; Bastiaens, L.; Russell, M.I.; Dickson, K.; Plant, S.; Ahad, J.M.E.; Newton, T.; Elliot, T.; Kalin, R.M. Ten year performance evaluation of a field-scale zero-valent iron permeable reactive barrier installed to remediate trichloroethene contaminated groundwater. *Environ. Sci. Technol.* **2010**, *44*, 3861–3869. [CrossRef]
8. Fu, F.; Dionysiou, D.D.; Liu, H. The use of zero-valent iron for groundwater remediation and wastewater treatment: A review. *J. Hazard. Mater.* **2014**, *267*, 194–205. [CrossRef]
9. Zingaretti, D.; Verginelli, I.; Baciocchi, R. Dehalogenation of trichloroethylene vapors by partially saturated zero-valent iron. *Sci. Total Environ.* **2019**, *647*, 682–689. [CrossRef]
10. Zingaretti, D.; Verginelli, I.; Luisetto, I.; Baciocchi, R. Horizontal permeable reactive barriers with zero-valent iron for preventing upward diffusion of chlorinated solvent vapors in the unsaturated zone. *J. Contam. Hydrol.* **2020**, *234*, 103687. [CrossRef]
11. Powell, R.M.; Blowes, D.W.; Gillham, R.W.; Schultz, D.; Sivavec, T.; Puls, R.W.; Vogan, H.L.; Powell, P.D.; Landis, R. Permeable reactive barrier technologies for contaminant remediation. In *US EPA*; 1998; Volume 600, pp. 1–94.
12. Duan, J.; Zhu, H.; Xu, F.; Zhao, J. A new approach to 4-chlorophenol dechlorination on monometallic copper compared to its Cu/Fe bimetallic system. *Chem. Eng. J.* **2016**, *304*, 282–288. [CrossRef]

13. Rodrigues, R.; Betelu, S.; Colombano, S.; Tzedakis, T.; Masselot, G.; Ignatiadis, I. In Situ Chemical Reduction of Chlorinated Organic Compounds. In *Environmental Soil Remediation and Rehabilitation*; Springer International Publishing: Cham, Switzerland, 2020; pp. 283–398.

14. Noubactep, C. On the operating mode of bimetallic systems for environmental remediation. *J. Hazard. Mater.* **2009**, *164*, 394–395. [CrossRef] [PubMed]

15. Venkateshaiah, A.; Silvestri, D.; Wacławek, S.; Ramakrishnan, R.K.; Krawczyk, K.; Saravanan, P.; Pawlyta, M.; Padil, V.V.T.; Černik, M.; Dionysiou, D.D. A comparative study of the degradation efficiency of chlorinated organic compounds by bimetallic zero-valent iron nanoparticles. *Environ. Sci. Water Res. Technol.* **2022**, *8*, 162–172. [CrossRef]

16. He, N.; Li, P.; Zhou, Y.; Ren, W.; Fan, S.; Verkhozina, V.A. Catalytic dechlorination of polychlorinated biphenyls in soil by palladium–iron bimetallic catalyst. *J. Hazard. Mater.* **2009**, *164*, 126–132. [CrossRef] [PubMed]

17. Cwiertny, D.M.; Bransfield, S.J.; Livi, K.J.; Fairbrother, D.H.; Roberts, A.L. Exploring the influence of granular iron additives on 1, 1, 1-trichloroethane reduction. *Environ. Sci. Technol.* **2006**, *40*, 6837–6843. [CrossRef] [PubMed]

18. He, F.; Li, Z.; Shi, S.; Xu, W.; Sheng, H.; Gu, Y.; Jiang, Y.; Xi, B. Dechlorination of excess trichloroethene by bimetallic and sulfidated nanoscale zero-valent iron. *Environ. Sci. Technol.* **2018**, *52*, 8627–8637. [CrossRef]

19. Lien, H.L.; Zhang, W.X. Nanoscale Pd/Fe bimetallic particles: Catalytic effects of palladium on hydrodechlorination. *Appl. Catal. B Environ.* **2007**, *77*, 110–116. [CrossRef]

20. Chao, K.P.; Ong, S.K.; Fryzek, T.; Yuan, W.; Braida, W. Degradation of trichloroethylene using iron, bimetals and trimetals. *J. Environ. Sci. Health Part A* **2012**, *47*, 1536–1542. [CrossRef]

21. Liu, X.; Wu, M.; Zhao, J. Removal of Trichloroethylene from Water by Bimetallic Ni/Fe Nanoparticles. *Water* **2022**, *14*, 1616. [CrossRef]

22. Ko, S.O.; Lee, D.H.; Kim, Y.H. Kinetic studies of reductive dechlorination of chlorophenols with Ni/Fe bimetallic particles. *Environ. Technol.* **2007**, *28*, 583–594. [CrossRef]

23. Huang, Y.Y.; Liu, F.; Li, H.D. Degradation of tetrachloromethane and tetrachloroethene by Ni/Fe bimetallic nanoparticles. In *Journal of Physics: Conference Series*; IOP Publishing: Bristol, UK, 2009; Volume 188, p. 012014.

24. Xu, F.; Deng, S.; Xu, J.; Zhang, W.; Wu, M.; Wang, B.; Huang, J.; Yu, G. Highly active and stable Ni–Fe bimetal prepared by ball milling for catalytic hydrodechlorination of 4-chlorophenol. *Environ. Sci. Technol.* **2012**, *46*, 4576–4582. [CrossRef]

25. Schrick, B.; Blough, J.L.; Jones, A.D.; Mallouk, T.E. Hydrodechlorination of trichloroethylene to hydrocarbons using bimetallic nickel−iron nanoparticles. *Chem. Mater.* **2002**, *14*, 5140–5147. [CrossRef]

26. Zhuang, M.; Shi, W.; Wang, H.; Cui, L.; Quan, G.; Yan, J. Carbothermal Synthesis of Ni/Fe Bimetallic Nanoparticles Embedded into Graphitized Carbon for Efficient Removal of Chlorophenol. *Nanomaterials* **2021**, *11*, 1417. [CrossRef] [PubMed]

27. Quan, X.; Liu, H.J.; Yang, F.L.; Xue, D.M.; Zhao, Y.Z. Dechlorination of three polychlorinated hydrocarbons in water using bemetallic systems. *China Environ. Sci.* **1998**, *18*, 333–336.

28. Sui, H.; Rong, Y.; Song, J.; Zhang, D.; Li, H.; Wu, P.; Shen, Y.; Huang, Y. Mechanochemical destruction of DDTs with Fe-Zn bimetal in a high-energy planetary ball mill. *J. Hazard. Mater.* **2018**, *342*, 201–209. [CrossRef] [PubMed]

29. Ruan, X.; Liu, H.; Wang, J.; Zhao, D.; Fan, X. A new insight into the main mechanism of 2, 4-dichlorophenol dechlorination by Fe/Ni nanoparticles. *Sci. Total Environ.* **2019**, *697*, 133996. [CrossRef] [PubMed]

30. Scaria, J.; Nidheesh, P.V.; Kumar, M.S. Synthesis and applications of various bimetallic nanomaterials in water and wastewater treatment. *J. Environ. Manag.* **2020**, *259*, 110011. [CrossRef] [PubMed]

31. Cook, S.M. Assessing the Use and Application of Zero-Valent Iron Nanoparticle Technology for Remediation at Contaminated Sites. Jackson State University. 2009. Available online: https://clu-in.org/download/studentpapers/zero-valent-iron-cook.pdf (accessed on 15 May 2022).

32. O'Carroll, D.; Sleep, B.; Krol, M.; Boparai, H.; Kocur, C. Nanoscale zero valent iron and bimetallic particles for contaminated site remediation. *Adv. Water Resour.* **2013**, *51*, 104–122. [CrossRef]

33. Guan, X.; Sun, Y.; Qin, H.; Li, J.; Lo, I.M.; He, D.; Dong, H. The limitations of applying zero-valent iron technology in contaminants sequestration and the corresponding countermeasures: The development in zero-valent iron technology in the last two decades (1994–2014). *Water Res.* **2015**, *75*, 224–248. [CrossRef] [PubMed]

34. Gunawardana, B.; Singhal, N.; Swedlund, P. Degradation of chlorinated phenols by zero valent iron and bimetals of iron: A review. *Environ. Eng. Res.* **2011**, *16*, 187–203. [CrossRef]

35. Doong, R.A.; Lai, Y.L. Effect of metal ions and humic acid on the dechlorination of tetrachloroethylene by zerovalent iron. *Chemosphere* **2006**, *64*, 371–378. [CrossRef]

36. Xiong, Z.; Lai, B.; Yang, P.; Zhou, Y.; Wang, J.; Fang, S. Comparative study on the reactivity of Fe/Cu bimetallic particles and zero valent iron (ZVI) under different conditions of N2, air or without aeration. *J. Hazard. Mater.* **2015**, *297*, 261–268. [CrossRef] [PubMed]

37. Liu, W.J.; Qian, T.T.; Jiang, H. Bimetallic Fe nanoparticles: Recent advances in synthesis and application in catalytic elimination of environmental pollutants. *Chem. Eng. J.* **2014**, *236*, 448–463. [CrossRef]

38. Zhang, S.S.; Yang, N.; Ni, S.Q.; Natarajan, V.; Ahmad, H.A.; Xu, S.; Fang, X.; Zhan, J. One-pot synthesis of highly active Ni/Fe nano-bimetal by simultaneous ball milling and in situ chemical deposition. *RSC Adv.* **2018**, *8*, 26469–26475. [CrossRef] [PubMed]

39. Azabou, M.; Gharsallah, H.I.; Escoda, L.; Suñol, J.J.; Kolsi, A.W.; Khitouni, M. Mechanochemical reactions in nanocrystalline Cu–Fe system induced by mechanical alloying in air atmosphere. *Powder Technol.* **2012**, *224*, 338–344. [CrossRef]

40. Moumeni, H.; Alleg, S.; Greneche, J.M. Structural properties of $Fe_{50}Co_{50}$ nanostructured powder prepared by mechanical alloying. *J. Alloys Compd.* **2005**, *386*, 12–19. [CrossRef]

41. Wille, C.G.; Kirchheim, R. Time evolution of morphology in mechanically alloyed Fe–Cu. *Ultramicroscopy* **2011**, *111*, 730–737. [CrossRef]

42. Hamzaoui, R.; Elkedim, O. Magnetic properties of nanocrystalline Fe–10% Ni alloy obtained by planetary ball mills. *J. Alloys Compd.* **2013**, *573*, 157–162. [CrossRef]

43. Zhu, H.; Xu, F.; Zhao, J.; Jia, L.; Wu, K. Catalytic hydrodechlorination of monochloroacetic acid in wastewater using Ni-Fe bimetal prepared by ball milling. *Environ. Sci. Pollut. Res.* **2015**, *22*, 14299–14306. [CrossRef]

44. Gheisari, K.; Javadpour, S.; Oh, J.T.; Ghaffari, M. The effect of milling speed on the structural properties of mechanically alloyed Fe–45% Ni powders. *J. Alloys Compd.* **2009**, *472*, 416–420. [CrossRef]

45. Brunauer, S.; Deming, L.S.; Deming, W.E.; Teller, E. On a theory of the van der Waals adsorption of gases. *J. Am. Chem. Soc.* **1940**, *62*, 1723–1732. [CrossRef]

46. Tee, Y.H.; Bachas, L.; Bhattacharyya, D. Degradation of trichloroethylene by iron-based bimetallic nanoparticles. *J. Phys. Chem. C* **2009**, *113*, 9454–9464. [CrossRef] [PubMed]

47. Alami, A.H.; Hawili, A.A. Synthesis, characterization and applications of FeCu alloys. *Appl. Surf. Sci. Adv.* **2020**, *1*, 100027. [CrossRef]

48. Eckert, J.; Holzer, J.C.; Krill, C.E., III; Johnson, W.L. Mechanically driven alloying and grain size changes in nanocrystalline Fe-Cu powders. *J. Appl. Phys.* **1993**, *73*, 2794–2802. [CrossRef]

49. Eckert, J.; Holzer, J.C.; Johnson, W.L. Thermal stability and grain growth behavior of mechanically alloyed nanocrystalline Fe-Cu alloys. *J. Appl. Phys.* **1993**, *73*, 131–141. [CrossRef]

50. Liu, Y.; Zhang, J.; Yu, L.; Jia, G.; Jing, C.; Cao, S. Magnetic and frequency properties for nanocrystalline Fe–Ni alloys prepared by high-energy milling method. *J. Magn. Magn. Mater.* **2005**, *285*, 138–144. [CrossRef]

51. Thommes, M.; Kaneko, K.; Neimark, A.V.; Olivier, J.P.; Rodriguez-Reinoso, F.; Rouquerol, J.; Sing, K.S. Physisorption of gases, with special reference to the evaluation of surface area and pore size distribution (IUPAC Technical Report). *Pure Appl. Chem.* **2015**, *87*, 1051–1069. [CrossRef]

52. He, F.; Gong, L.; Fan, D.; Tratnyek, P.G.; Lowry, G.V. Quantifying the efficiency and selectivity of organohalide dechlorination by zerovalent iron. *Environ. Sci. Process. Impacts* **2020**, *22*, 528–542. [CrossRef]

53. Thermo Environmental Instruments. TVA 1000 response factors. P/N 50039. 2000. Available online: https://tools.thermofisher.com/content/sfs/manuals/EPM-manual-TVA2020.pdf (accessed on 15 May 2022).

54. Campbell, T.J.; Burris, D.R.; Roberts, A.L.; Wells, J.R. Trichloroethylene and tetrachloroethylene reduction in a metallic iron–water-vapor batch system. *Environ. Toxicol. Chem. Int. J.* **1997**, *16*, 625–630.